Control of the conformations of ion Coulomb crystals in a Penning trap

R. C. Thompson, S. Mavadia, J. F. Goodwin, G. Stutter, S. Bharadia, D. R. Crick, and D. M. Segal

Citation: AIP Conference Proceedings **1668**, 040003 (2015); doi: 10.1063/1.4923116
View online: https://doi.org/10.1063/1.4923116
View Table of Contents: http://aip.scitation.org/toc/apc/1668/1
Published by the American Institute of Physics

Control of the Conformations of Ion Coulomb Crystals in a Penning Trap

R. C. Thompson, S. Mavadia, J. F. Goodwin, G. Stutter, S. Bharadia, D. R. Crick and D. M. Segal

Blackett Laboratory, Imperial College London, London SW7 2AZ, UK

Abstract. Ion Coulomb crystals containing small numbers of ions have been created and manipulated in a wide range of configurations in a Penning trap, from a linear string, through various three-dimensional conformations, to a planar crystal. We show that the dynamics of the system simplifies enormously in a frame which rotates at half the cyclotron frequency and we discuss the effect of the radial cooling laser beam in this frame. Simulations show that the crystal conformations can be reproduced by finding the minimum energy configuration in a frame whose radial potential is modified by the rotation of the ion crystal. The rotation frequency of the crystal deduced from the simulations is consistent with the known laser parameters. We also show that even though the number of ions in our system is small (typically less than 20), the system still behaves like a plasma and its static properties can be calculated using the standard model for a single-component plasma in a trap.

Keywords: Penning trap, single-component plasma, Coulomb crystal, laser cooling, nonneutral plasma
PACS: 37.10.Rs, 37.10.Ty, 52.27.Aj,57.27.Jt

INTRODUCTION

Penning traps have been used for a wide range of experiments in precision measurements, plasma physics, atomic physics and quantum optics (see for example [1, 2]). Just as ion Coulomb crystals (ICC) are formed in radiofrequency (RF) traps under the effect of laser cooling, the same processes occur in Penning traps. However, the properties of the Penning trap, in particular the negative total energy of the magnetron motion and the rotation of the ion crystal, complicate the observation of Coulomb crystals in this type of trap. Experiments that have been carried out with ICC in Penning traps generally make use of large numbers of ions (see for example [3, 4]).

Small ICC have applications in the areas of quantum information processing and quantum simulation, for example in the simulation of spin frustration in a three-ion system [5]. The Penning trap may offer advantages for this type of work, due to the fact that it allows ICC to be prepared in a variety of one-, two-, and three-dimensional conformations with known symmetries. In order to investigate these applications of ICC, it is necessary to control the conformation of the ICC and also to prepare the system in its ground state.

In this article we first discuss the background to the formation of ion Coulomb crystals in a Penning trap, then we show how the dynamics of the system can be described in an intuitive way in a frame rotating at half the cyclotron frequency. We then present our observations of such crystals at Imperial College London and discuss briefly how the system still behaves like a plasma despite the small number of particles present. Finally, we present our demonstration of optical sideband cooling to the quantum mechanical ground state of the axial motion of a single ion in our trap. This work paves the way towards new applications for small ICC in a Penning trap.

COULOMB CRYSTALS IN A PENNING TRAP

The Penning trap is an excellent device for confining atomic ions because the confinement is provided solely by static fields and the ions are well isolated from the environment. Axial confinement is provided by a positive potential on the endcaps, giving rise to axial oscillations at an angular frequency of $\omega_z = (4eV/mR^2)^{1/2}$ where e and m are the charge and mass of the ions, V is the applied voltage, and R is a constant related to the dimensions of the trap [6]. Radial confinement is achieved by the application of a static magnetic field along the axis of the trap, and gives rise to a motion which is a superposition of two radial oscillation frequencies. The first, ω_c', is called the modified cyclotron frequency and is equal to $\omega_c/2 + \omega_1$ where $\omega_c = eB/m$ is the pure cyclotron frequency corresponding to the magnetic

Non-Neutral Plasma Physics IX
AIP Conf. Proc. 1668, 040003-1–040003-8; doi: 10.1063/1.4923116

field B, and ω_1 is related to the cyclotron and axial frequencies through

$$\omega_1^2 = \omega_c^2/4 - \omega_z^2/2. \tag{1}$$

The other radial frequency is called the magnetron frequency and is given by $\omega_m = \omega_c/2 - \omega_1$. The total energy of the magnetron mode is negative due to the fact that the radial potential energy is negative. This makes the magnetron motion unstable, however, the ions may nevertheless be confined for long periods under ultrahigh vacuum (UHV) conditions.

If the temperature of the trapped ions is reduced far enough, it is possible for an ion Coulomb crystal to form [7]. The so-called Coulomb coupling parameter, $\Gamma = e^2/4\pi\varepsilon_0 a_{WS} kT$, is defined to be the ratio of the Coulomb interaction energy between nearest neighbours to the thermal energy. Crystallisation takes place when this parameter becomes greater than about 178 for a large number of particles. Here a_{WS} is the Wigner-Seitz radius, defined by $4\pi a_{WS}^3 n/3 = 1$, with n being the number density of the plasma. Such crystals were first reported in a Penning trap by the NIST group in 1988 [8]. Later experiments revealed the structure of the crystals by Bragg scattering of the laser light [3].

Unlike in a radiofrequency trap, the ion crystal in a Penning trap always rotates. This is a consequence of the Lorentz force arising from the presence of the magnetic field B. However, the rotation frequency, ω_R, is not fixed, taking a range of values between ω_m and ω_c'. As is well known, the rotation frequency is linked to the number density of the plasma or crystal through [2]

$$n = 2\varepsilon_0 m\omega_R(\omega_c - \omega_R)/e^2. \tag{2}$$

THE ROTATING FRAME

It is convenient to consider the formation of the ion crystal in a frame which rotates at half the cyclotron frequency, $\omega_c/2$. In this frame the Coriolis force cancels out the Lorentz force due to the magnetic field, so the particles behave as if they are in a modified electrostatic potential with no magnetic field present. The axial potential is unaffected by this transformation and it is easy to show that the effective radial potential is now a quadratic potential well with a characteristic frequency of ω_1 as defined in Equation (1) above [9].

The motion of a single ion in the rotating frame is easily related to the observed motion in the laboratory. Rotation at $+\omega_1$ becomes the cyclotron motion at $\omega_c/2 + \omega_1$ and rotation at $-\omega_1$ becomes the magnetron motion at $\omega_c/2 - \omega_1$.

For a cold ion plasma which has condensed into a Coulomb crystal, the lowest energy state in the rotating frame is when the crystal is stationary at the centre of the trap. It then has the maximum possible density and when observed from the laboratory frame it is rotating at $\omega_c/2$. This corresponds to Brillouin flow. Since the effective confining potential in the rotating frame corresponds to oscillation frequencies of ω_z in the axial direction and ω_1 in the two radial directions, the ion number density, n, is given by

$$n = m(\omega_z^2 + 2\omega_1^2)\varepsilon_0/e^2 = m\omega_c^2\varepsilon_0/2e^2 \tag{3}$$

which is the usual expression for the density at Brillouin flow.

It is also possible for the crystal to rotate as a solid body at a constant rate (say ω_R') in the rotating frame. This will normally be in the negative sense (the same direction as the magnetron motion) and will result in a rotation frequency as seen in the laboratory frame of $\omega_R = \omega_c/2 - \omega_R'$. This rotation frequency ω_R' can take any value between $+\omega_1$ and $-\omega_1$.

In the rotating frame, the density of the crystal will be reduced as a result of its rotation (i.e. the centrifugal force). This can be described as a reduction in the confining potential as seen by the rotating crystal. The new effective confining potential, ω_2, is given by $\omega_2^2 = \omega_1^2 - {\omega_R'}^2$. The parameters of the crystal (i.e., its density and aspect ratio) are therefore determined by its rotation frequency and the density is now given by

$$n = m(\omega_z^2 + 2\omega_2^2)\varepsilon_0/e^2. \tag{4}$$

Using the definition of ω_2 above, this can be re-expressed as

$$n = 2m\omega_R(\omega_c - \omega_R)\varepsilon_0/e^2, \tag{5}$$

in accordance with the usual formula given above for the plasma density in terms of the rotation frequency in the laboratory frame (Equation (2)).

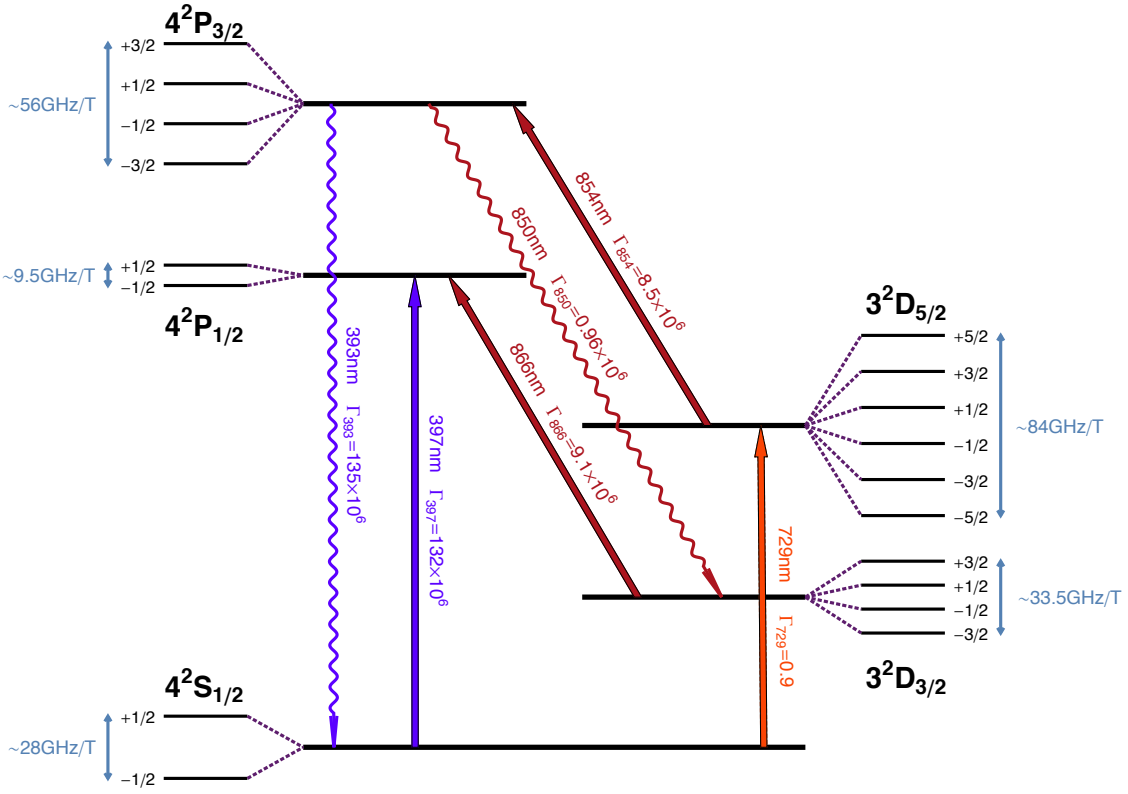

FIGURE 1. Energy level diagram for Ca^+. The magnetic field splittings are shown greatly exaggerated. Lasers are required at the wavelengths indicated with solid lines.

LASER COOLING

Doppler laser cooling can be used to reduce the temperature of a single trapped ion to the mK region. However, care has to be taken because the unstable nature of the magnetron motion means that it is heated rather than cooled if a radial cooling beam is simply directed through the centre of the trap. This can be overcome by offsetting the laser beam from the centre of the trap so that there is a gradient of laser intensity at the position of the ion [10, 11], or by applying the axialisation technique [12]. Alternatively, a rotating wall potential can be applied to the trap when more than one ion is present [13, 14]. The general effect of these techniques is to supply angular momentum to the system, forcing the orbits of the ions to become smaller, thus reducing the kinetic energy of the system.

In our experiment we use conventional radial and axial laser cooling without any additional fields. In general, laser cooling gives rise to a damping force that simply reduces the velocity of the particles. However, as mentioned above, the radial laser beam has to be offset from the centre of the Penning trap in order to cool all degrees of freedom of the ions. For small numbers of ions, the offset is comparable to the width of the laser beam. As a result, there is an approximately linear gradient of laser intensity across the centre of the trap. It can be shown that this, combined with the laser frequency detuning required for laser cooling, corresponds to a rotation of the damping force from the laser. This rate of rotation is proportional to the slope of laser intensity and in order to successfully cool both the magnetron and the cyclotron motions, it has to fall between the magnetron frequency and the modified cyclotron frequency [11, 15].

In our experiment the rotation of the crystal is determined by the parameters of the radial laser beam used for laser cooling, because of the absence of other effects. However, since we do not know the laser beam parameters sufficiently well, we have to determine the crystal rotation frequency indirectly, using simulations of the crystal behaviour.

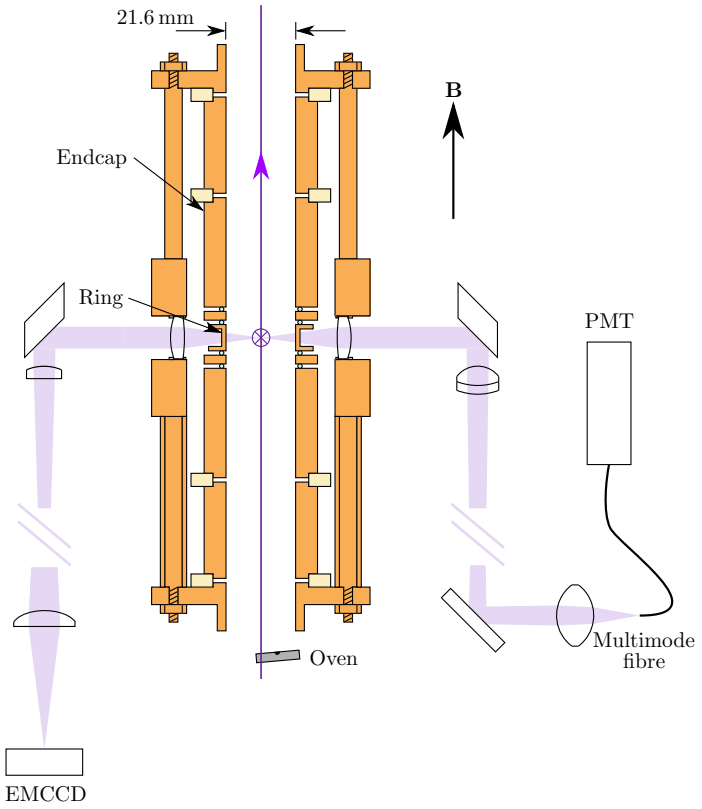

FIGURE 2. Schematic diagram of the Penning trap layout showing cooling laser beams and fluorescence detection optics. A cross-section of the cylindrical electrodes is shown. The vertical purple line is the axial laser cooling beam. The radial cooling beam passes through holes in the ring electrode, points into the page and is marked with a purple cross. The path taken by the atomic fluorescence is indicated by light purple shading. The internal diameter of the trap is 21.6 mm. The trap, vacuum enclosure (not shown) and beam-steering optics fit inside the 105-mm vertical bore of the superconducting magnet. EMCCD, electron multiplying charge-coupled device; PMT, photomultiplier tube [16].

EXPERIMENT

Our experiments with ion Coulomb crystals are described in detail in [16].

We work with singly-charged $^{40}Ca^{+}$ ions. Due to the presence of the 1.85 T magnetic field, all the energy levels of the ion are split by many GHz. This complicates the experimental requirements considerably as it means that many distinct laser wavelengths are required. The energy level diagram is shown in Figure 1. For effective cooing, we require two lasers at 397 nm, four laser frequencies at 866 nm (provided from a single laser using a high-frequency fibre electro-optic modulator), six laser frequencies at 854 nm (provided by a second laser using the same modulator), and one highly-stabilised laser operating at 729 nm for spectroscopy of the narrow qubit transition to the metastable $D_{5/2}$ state. The 854-nm laser is required for two reasons: firstly because rare decays are possible from the $P_{1/2}$ level to the $D_{5/2}$ level due to magnetic field induced mixing of the two D levels and also the two P levels [17], and secondly because optical sideband cooling on the 729 nm transition requires the $D_{5/2}$ state to be quenched.

A schematic diagram of the trap is shown in Figure 2. There are laser cooling beams both along the trap axis and in the radial plane. This ensures that all degrees of freedom of the ions are cooled effectively. The radial beam is offset from the centre of the trap as described above. The resulting laser intensity gradient determines the rotation frequency of the crystal, but although it can be estimated from the laser parameters, it is not known precisely. The ion crystal is imaged from the side (perpendicular to the magnetic field direction) on an EMCCD camera and therefore the rotation of the ion crystal leads to the image of any off-axis ion being smeared into a line. This can be seen in Figure 3 which shows on the left an image of two ions aligned along the vertical trap axis and on the right the same two ions lying in

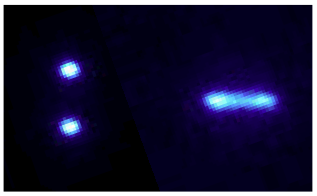

FIGURE 3. Two images of two ions aligned along (left) or perpendicular (right) to the vertical trap axis. The separation of the two ions on the left is approximately 30 μm. When the ions are aligned perpendicular to the trap axis, their rotation about the trap axis leads to the image becoming a line rather than separated points.

the radial plane.

Using this system we are able to trap and image up to approximately 30 ions in a chain along the axis of the trap when we use a low trapping voltage (see [16]). At higher trapping voltages, the ions form into three-dimensional Coulomb crystals and we are able to manipulate the conformation of the ion Coulomb crystal by varying the trapping voltage. At the highest voltages the crystal forms a two-dimensional sheet, as employed by the NIST group in their experiments [4]. A representative series of images of a crystal containing 15 ions is shown in Figure 4. Each of the images obtained experimentally on the left of each pane is compared to a computer simulation on the right of each pane. The simulation program finds the lowest energy configuration of the ions in a three-dimensional ellipsoidal potential well by starting from an initial random arrangement of ions and iteratively moving each ion in the direction of the total force acting on it from all the other ions and the trapping fields, until equilibrium is reached. A simulated image is formed by performing an angular average and taking into account the finite imaging resolution of the optical system. This can then be compared visually with the experimental image. In the simulation, the axial potential is known from the applied trapping voltage. At Brillouin flow, the effective radial potential is only determined by the trapping voltage, but this is modified if the crystal is rotating relative to the rotating frame, as it is expected to because of the interaction with the offset radial cooling beam. A comparison of each image with simulations obtained for different effective radial potentials therefore allows us to determine the rotation speed of the crystal in each of the images.

The comparison of the experimental images with the computer simulations shows that all the observed crystal conformations are reproduced well in the simulations. Moreover, the crystal rotation speed which is determined in this way from the simulations is roughly constant for different crystal conformations and trapping voltages. In Figure 4 this value is approximately $\omega_c/4$, which is consistent with an estimate based on the known radial cooling laser beam parameters [16].

It is possible to calculate the aspect ratio and energy expected for a cold plasma in equilibrium in an ellipsoidal potential [18]. It is perhaps remarkable how the parameters obtained in this manner match those obtained from simulations of ion Coulomb crystals, even for a small number of ions. Figure 5 shows the energies of various simple configurations of a crystal containing just four ions. The system will always adopt the configuration with the lowest total energy. In the case of four ions, the transition from one configuration to the next as the trapping potential is changed is always continuous. If the energy of a plasma containing the same total amount of charge in the same trapping potential is calculated, a very similar variation with trapping potential is found. Even though there are only four particles present, the energy calculated for the plasma is less than a factor of 2 larger than that found for the crystal. Similar calculations with larger numbers of ions give a much closer agreement, as would be expected. A comparison of the plasma and crystal aspect ratios shows that these are also very similar, even for the four-ion case. It is therefore clear that the static properties of the crystal are surprisingly well represented by calculations using a standard plasma model, even when the crystal only contains a very small number of ions.

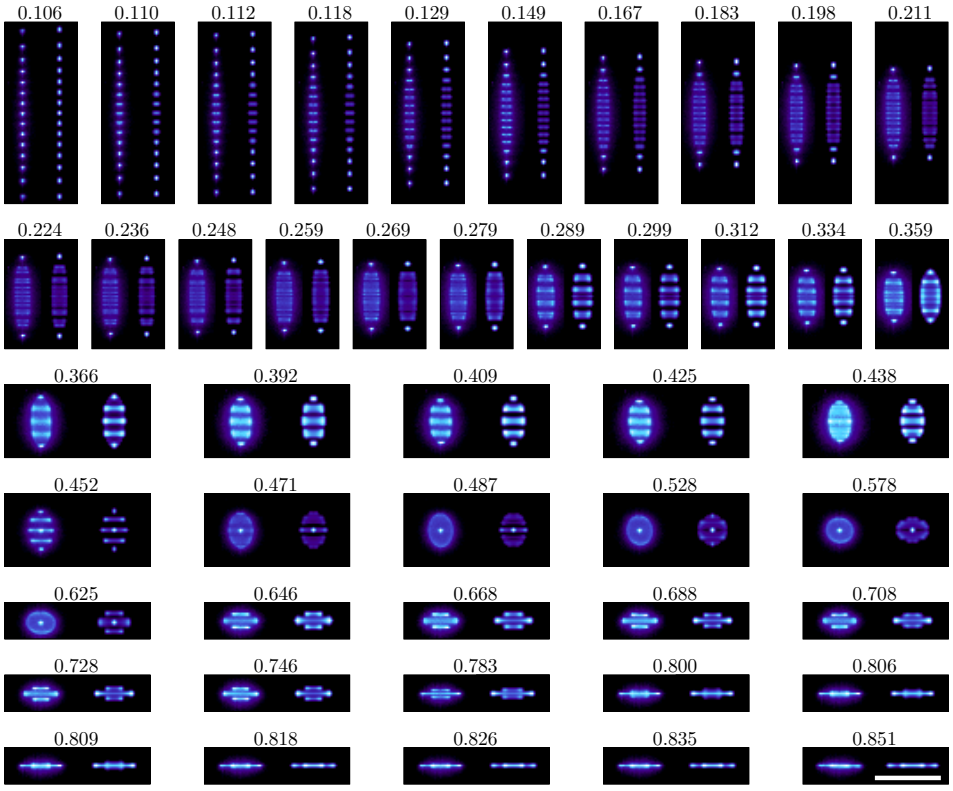

FIGURE 4. Experimentally obtained images of 15-ion crystals for different axial potentials (left of each panel), compared with computer simulations (right of each panel). By increasing the axial confinement, a linear string is transformed into a zigzag structure, then a 3D crystal and finally a planar structure. Each image is labelled with the value of the normalized axial trapping frequency (the trap becomes unstable when this quantity is equal to unity). There is a 100-μm scale bar in the bottom right-hand pane, which applies to all the images [16].

OPTICAL SIDEBAND COOLING

We have also recently demonstrated optical sideband spectroscopy of a single ion in the Penning trap [19]. For this work we use a narrow-band laser at 729 nm which drives the electric quadrupole transition from the $S_{1/2}$ ground state to the $D_{5/2}$ metastable state. The ion is pre-cooled using Doppler cooling lasers as described above, for a period of a few ms. After this the cooling lasers are turned off and the ion is probed with the 729 nm laser for typically 40 μs. The cooling lasers are then turned back on and the first few ms of fluorescence is recorded. If the ion was shelved in the $D_{5/2}$ state, then there there is no fluorescence initially. At each laser frequency we repeat this measurement cycle 100 to 400 times in order to obtain the probability of excitation to the metastable level. A plot of this probability as a function of probe laser frequency shows motional sidebands in the spectrum as expected. Figure 6 shows a typical spectrum for the axial motion obtained in this way. We have also been able to measure spectra of the radial motion of the ion, which show sidebands due to both the cyclotron and the magnetron motions [19]. These spectra demonstrate that the temperature of the magnetron motion is of the order of tens of microkelvin, much lower than the standard Doppler limit. This is another consequence of the unusual nature of the magnetron motion and in particular the low rate of cooling of this motion, even with the offset radial cooling beam [10].

In later work we have also demonstrated optical sideband cooling to the ground state of the axial motion of an ion in a Penning trap for the first time [20]. The measured heating rate in these experiments was found to be very low compared to most measurements in RF traps at room temperature. This is expected because the trap is large compared to typical RF traps, and therefore heating mechanisms related to patch potentials on the electrode surfaces are much less important.

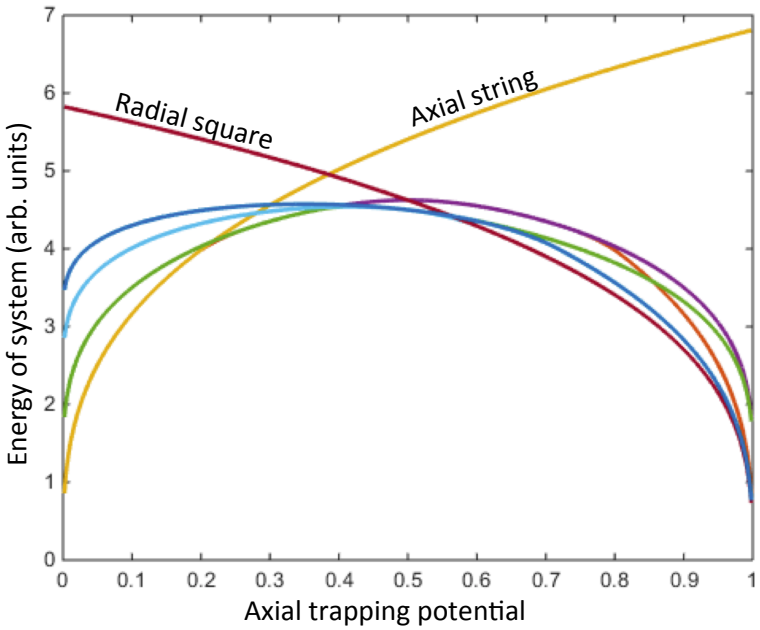

FIGURE 5. Plots of the total energy of the crystal for several different configurations of four ions as a function of the relative strength of the axial and radial trapping potentials. For any given combination of trapping potentials, the configuration adopted by the crystal will be that with the lowest energy. As expected, low axial trapping strength leads to the ions forming an axial string and if the axial trapping strength is high the ions form a square in the radial plane. For intermediate trapping strengths, other two and three dimensional structures such as a diamond or a tetrahedron are favoured energetically.

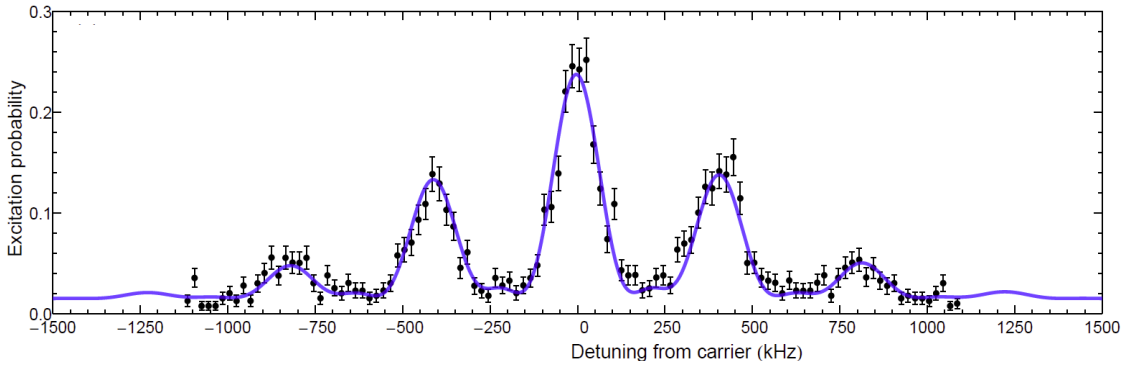

FIGURE 6. Optical sideband spectrum of the axial motion of a single ion in a Penning trap after Doppler cooling, recorded at a trap potential of 240 V. The solid line is a fit to the full quantum dynamics of the system and corresponds to a temperature of T= 0.47 $\pm$ 0.04 mK ($\bar{n} = 24 \pm 2$). The error bars reflect the statistical uncertainty in the shelving probability arising from the number of repetitions of the measurement cycle at each frequency step [19].

CONCLUSIONS

We have made an extensive study of the properties of Coulomb crystals of ions in a Penning trap. We are able to control the conformation of the crystal over a wide range by varying the trapping potential. The rotation frequency of the crystal can be estimated by matching the image of the crystal to simulations that take into account the effect of the rotation on the radial trapping potential. The observed phenomena can be understood in a simple way by transforming to a frame that rotates at half of the pure cyclotron frequency. We also find that the crystal energy and aspect ratio obtained from simulations with small numbers of ions match surprisingly well with those calculated for a plasma held in the same potential. Finally, we have demonstrated optical sideband spectroscopy and optical sideband cooling of a single ion in a Penning trap for the first time. The low heating rate found in these measurements points to the potential for the use of ions in a Penning trap for applications in quantum information processing or quantum thermodynamics.

ACKNOWLEDGMENTS

This work was supported by the UK Engineering and Physical Sciences Research Council (EP/D068509/1) and by the European Commission STREP PICC (FP7 2007-2013 Grant number 249958). We gratefully acknowledge financial support towards networking activities from COST Action MP 1001: Ion Traps for Tomorrows Applications. We also gratefully acknowledge J. Hwang for the loan of the electron multiplying charge-coupled device camera.

REFERENCES

1. K. Blaum, Y. N. Novikov, and G. Werth, *Contemporary Physics* **51**, 149 (2010).
2. J. J. Bollinger, J. N. Tan, W. M. Itano, D. J. Wineland, and D. H. E. Dubin, *Physica Scripta* **T59**, 352 (1995).
3. J. N. Tan, J. J. Bollinger, B. Jelenkovic, and D. J. Wineland, *Phys. Rev. Lett.* **75**, 4198 (1995).
4. B. C. Sawyer, J. W. Britton, A. C. Keith, C. C. J. Wang, J. K. Freericks, H. Uys, M. J. Biercuk, and J. J. Bollinger, *Phys. Rev. Lett.* **108**, 213003 (2012).
5. K. Kim, M. S. Chang, S. Korenblit, R. Islam, E. E. Edwards, J. K. Freericks, G. D. Lin, L. M. Duan, and C. Monroe, *Nature* **465**, 590 (2010).
6. G. Z. K. Horvath, R. C. Thompson, and P. L. Knight, *Contemporary Physics* **38**, 25 (1997).
7. R. C. Thompson, *Contemporary Physics* **56** (2015).
8. S. L. Gilbert, J. J. Bollinger, and D. J. Wineland, *Phys. Rev. Lett.* **60**, 2022 (1988).
9. R. C. Thompson, and D. C. Wilson, *Zeitschrift Fur Physik D-Atoms Molecules and Clusters* **42**, 271 (1997).
10. W. M. Itano, and D. J. Wineland, *Phys. Rev. A* **25**, 35 (1982).
11. R. C. Thompson, and J. Papadimitriou, *Journal of Physics B – Atomic Molecular and Optical Physics* **33**, 3393 (2000).
12. R. J. Hendricks, E. S. Phillips, D. M. Segal, and R. C. Thompson, *Journal of Physics B-Atomic Molecular and Optical Physics* **41** (2008).
13. X. P. Huang, J. J. Bollinger, T. B. Mitchell, and W. M. Itano, *Phys. Rev. Lett.* **80**, 73 (1998).
14. S. Bharadia, M. Vogel, D. M. Segal, and R. C. Thompson, *Applied Physics B – Lasers and Optics* **107**, 1105 (2012).
15. M. Asprusten, S. Worthington, and R. C. Thompson, *Applied Physics B – Lasers and Optics* **114**, 157 (2014).
16. S. Mavadia, J. F. Goodwin, G. Stutter, S. Bharadia, D. R. Crick, D. M. Segal, and R. C. Thompson, *Nature Communications* **4**, 2571 (2013).
17. D. R. Crick, S. Donnellan, D. M. Segal, and R. C. Thompson, *Phys. Rev. A* **81**, 052503 (2010).
18. Y. Kiwamoto, J. Aoki, and Y. Soga, *Phys. Plasmas* **11**, 4868 (2004).
19. S. Mavadia, G. Stutter, J. F. Goodwin, D. R. Crick, R. C. Thompson, and D. M. Segal, *Phys. Rev. A* **89**, 032502 (2014).
20. J. F. Goodwin, G. Stutter, R. C. Thompson, and D. M. Segal (2014), URL `http://arxiv.org/abs/1407.6121`.